A Dynamic Optimal Battery Swapping Mechanism for Electric Vehicles using an LSTM-based Rolling Horizon Approach

Ahmed A. Shalaby, Mostafa F. Shaaban, *Senior Member, IEEE*, Mohamed Mokhtar, *Member, IEEE*, Hatem H. Zeineldin, *Senior Member, IEEE* and Ehab F. El-Saadany, *Fellow, IEEE.*

***Abstract*—This paper proposes a new approach for optimal operation of an Electric Vehicle (EV) battery-swapping station (BSS) based on Rolling-Horizon optimization (RHO). The BSS has several swapping bays such that each can accommodate an EV for swapping single or multiple battery units. The proposed BSS model considers serving different types of EVs using a heterogeneous battery stock. The charging of the depleted batteries (DBs) is performed using continuously controlled variable chargers which makes it more flexible for providing grid services. While previous studies focused on day-ahead modeling of BSSs, our study considers BSS dynamic scheduling. The goal is to maximize the daily profit using an RHO mechanism to provide optimal swapping and charging/discharging processes. The problem is defined as mixed-integer nonlinear programming (MINLP), then it's linearized into a mixed-integer linear problem (MILP) to reduce the computational complexity. To predict the EV's swapping demand, a long short-term memory (LSTM) recurrent neural network is utilized as a time series forecasting engine. The proposed model is validated through a set of case studies comparing the LSTM-based RHO mechanism versus unscheduled operation and day-ahead scheduling. Simulation results demonstrate that the proposed dynamic scheduling mechanism increases the profit between 10% and 25.7% compared to the day-ahead scheduling. Furthermore, the number of EVs served using the proposed approach increases between 11% and 14% compared to the day-ahead model.**

***Index Terms*— Battery swapping stations, battery to grid, EV charging stations, electric vehicles, LSTM, MILP, rolling-horizon optimization.**

NOMENCLATURE

A. Acronyms

BSS	Battery Swapping Station
B2G	Battery to Grid
B2B	Battery to Battery
DB	Depleted Battery
FCBI	Fully Charged Battery Inventory
G2B	Grid to Battery
RHO	Rolling Horizon Optimization
SOC	State of Charge

B. Sets:

B	Set of batteries
K	Set of chargers
T	Set of time slots
T_{β}^{arv}	A subset of time slots for the EV arrivals at each bay β
$T_{\beta}^{arv'}$	A complementary subset representing the time slots without EV arrivals at each bay β
$T'_{m,\beta}$	A subset of time slots T representing the time slots at which there are no EV arrivals requesting type m batteries at bay β
U	Set of swapping bays
ψ_m	Group of the set B representing batteries of type-m
λ_j	Group of the set K representing chargers of group-j

C. Parameters:

c_{τ}^{gr}	Time-of-use electricity price in ¢/kWh
c^{kWh}	Price of the energy swapped in ¢/kWh
C_b^{swap}	Fixed price in cents for replacing battery b
C^{DEG}	Cost of battery degradation
$\mathcal{C}_b$	Charging/discharging cycles of each battery
DOD^{max}	Maximum depth of battery discharge in %
e_b^{max}	Maximum capacity of battery b in kWh
ω	A percentage shaping the charging characteristics
$N_{\tau,\beta}^{units}$	The number of battery units requested by an EV
N_j^{ch}	The number of chargers available in group j
p_c^{MAXd}	Maximum battery discharging rate in kW
p_c^{MAXc}	Maximum battery charging rate in kW
P^{MAX-TF}	The power limit from/to the grid through the power transformer in kVA
$soc_{\tau,\beta}^{ev}$	State of charge of the arriving EVs DBs at time τ and bay β
soc_b^0	Initial SOC of each battery at the beginning of the simulation
soc_b^{max}	Maximum SOC of any battery b
ζ	A percentage of the maximum battery capacity
Δsoc_b^{deg}	Degradation in the battery SOC
Δt	The time step in hours
η^{ch}	The efficiency of charging
η^{dch}	The efficiency of discharging

A.A. Shalaby and M.F. Shaaban are with the Department of Electrical Engineering, American University of Sharjah, Sharjah, United Arab Emirates (e-mail: b00086255@alumni.aus.edu and mshaaban@aus.edu).

M. Mokhtar is with the Department of Electrical Power and Machines, Ain Shams University, Cairo, Egypt (e-mail: m.mokhtar@eng.asu.edu.eg).

H. H. Zeineldin is with the Electrical Power and Machines Department, Faculty of Engineering, Cairo University, Giza, Egypt, and currently on leave from Khalifa University, Abu Dhabi, UAE (e-mail: hatem.zeineldin@ku.ac.ae)

E. F. El-Saadany, Director of the Advanced Power and Energy Center, EECS Department, Khalifa University, Abu Dhabi, UAE (e-mail:ehab.elsadaany@ku.ac.ae).

This work was supported by the American University of Sharjah under Grant FRG19-L-E37 and in part, the theory development was supported by project CIRA-013-2020, Khalifa University.

https://doi.org/10.1109/TITS.2021.3138892

μ_b^{deg}	Battery degradation price

D. Variables:

C^{G2B}	Cost of purchasing energy from the grid
$ch_{\tau,b}$	Charging status of battery b at time τ (1 if charging, 0 otherwise)
$M_{\tau,\beta}$	Decision binary variable for serving an EV at time τ and bay β (1 if served, 0 otherwise)
$\mathcal{N}^{BAT-SW}$	The total number of batteries swapped at the BSS
$\mathcal{N}^{served}$	The total number of EVs served at the BSS
O	The total profit of the BSS. (objective function variable)
$p_{\tau,b}^{ch}$	Charging power of battery b during time slot τ
$p_{\tau,b}^{dch}$	Discharging power of battery b during time slot τ
P_{τ}^{net-TF}	The net power flow through the BSS transformer
R^{S}	Revenue from swapping
R^{B2G}	Revenue from selling energy to the grid
$soc_{\tau,b}$	State of charge of battery b at the end of time slot τ
$\Delta soc_{\tau,b}^{swap}$	The difference in SOC between a customers' DB and the swapped charged battery
$sw_{\tau,b,\beta}$	Swapping status of battery b at time τ and bay β (1 if swapped, 0 otherwise)
$z_{\tau,b,\beta}$	Intermediate variable replacing the product of a binary variable and a positive variable

E. Indices:

b	Index of batteries
c	Index of chargers
j	Index of the group of chargers
m	Index of battery type
β	Index of swapping bays
τ	Index of time

I. Introduction

The future of Electric vehicles (EVs) is evolving rapidly, due to the impact of EVs on reducing greenhouse emissions and reliance on fossil fuels. The number of EVs in the United States is expected to reach 18.7 million by 2030 that is 7 % of the expected available vehicles on road in 2030 [1]. Some governments have already taken action to revolutionize their roads. The UK government has launched a plan named ‘road to zero’ such that all the vehicles on the roads will be zero emissions by 2040 [2]. However, there are still some factors affecting the fast deployment of EVs, such as the availability of the EV charging infrastructure [3], the EV's limited driving range, and the EV charging time. Some companies have already started to produce EVs with an extended driving range (e.g., Tesla Model S “402 miles” and Tesla Model 3 “322 miles” [4]). The fact is that in real-world usage this range is much lesser. Nowadays, two methods have been proposed to extend the EV driving range: battery swapping stations (BSS) and EV hybridization with an internal combustion engine vehicle [5]. In this research, our main focus is to tackle the issue of the EV's long charging times by using battery swapping stations.

The idea of the BSS is based on replacing an EV depleted battery (DB) with a charged one in just a few minutes. Compared to charging EVs at charging stations, the BSS provides a much faster alternative service. For instance, it would take a fast-charging station around 80 minutes to fully charge the Tesla Model S battery [6]. Whereas, it takes only 12 minutes to swap a battery in a typical EV BSS in Shandong province of China [7]. It can be noticed that the BSS is being recently introduced in the literature and in the market due to its tremendous benefits. In [8] the authors focused only on the business aspect of the BSS. In fact, this technology requires an operational model in order to provide optimal scheduling for it and to generate profits while meeting the swapping demand. The main idea is to design the BSS station and model its daily operation as in [9] and [10]. Furthermore, this could be developed into a BSS planning model over multiple years as in [11]. The BSS is also capable of providing grid ancillary services such as discharging to the grid. This can be typically done by scheduling the charging/discharging of the BSS based on the electricity prices [12]. In this regard, the BSS sells electricity at high prices during the day and purchase it at a low price while meeting the swapping demand.

Some studies considered the operation of the BSS with renewable generation to minimize the operational costs as shown in [10], [13], and [14]. In [10] the authors highlight the impact of introducing PV-based BSS systems on the BSS daily profit. Researchers in [13] proposed a model for a BSS coupled with PV generation and the power grid considering the uncertainties from the swapping demand and PV generation. A PV-based BSS is modeled in [14] by considering the service availability and self-consumption of PV. Regardless of the impact of PV on reducing operational costs, these studies ignored the difficulty of installing renewable energy infrastructures in urban cities. Also, few BSS models studied the BSS operation while coupled with a micro-grid (MG). In [15] the authors considered the conflicting objectives of the MG and the BSS. Recently, Mingfei Pan has incorporated a BSS with networked nano-grids [16].

Most of the BSS models considered that charging of the batteries occurs at the BSS station. However, some researchers combined both operations of BSS and battery charging stations (BCS). In [17], the BSS is only used as a store, and DBs are charged at a BCS before being delivered to the BSS. To combine both BSS and BCS operations, modeling the transportation system for the batteries is required. In this paper, the charging of the batteries is done locally at the BSS, thus, modeling of the battery logistics is not needed. The BSS models presented in the literature were not limited to electric cars only. In [7] an operation model for a BSS serving electric buses is proposed. Whereas, in [6] a study has been investigated on a BSS serving electric taxis only in an urban city. The model in [6] is based on some unrealistic assumptions, for instance, it was assumed that the BSS is operating only from 9.00 a.m. to 8.00 p.m., thus, limiting its operation. Hence, the BSS proposed in this paper is operating during the whole day and it’s capable of serving several types of EVs. Many authors considered a constant charging rate in the modeling of BSS systems. Undoubtedly, the usage of constant rate chargers that are controlled using conventional on/off control techniques is easier to be modeled. Very few works utilized continuously controlled chargers, which makes it more flexible to provide grid services [18]. Therefore, a combination of variable rate charging and the battery charging characteristics are accounted

into our proposed model. In [19] different charging control methods have been proposed considering providing ancillary services to the grid.

BSS scheduling and operation is presented as a large size mixed-integer nonlinear optimization problem (MINLP). Recently, heuristic optimization algorithms have shown reasonable results in solving such problems as shown in [9], [11], and [20]. The authors in [9] developed an integrated algorithm that is used to solve the optimization problem of a BSS using genetic algorithms (GA), particle swarm optimization (PSO), and differential evolution (DE). In [11] a heuristic technique is used to solve the optimization problem using differential evolution enhanced by fitness sharing which is faster to solve compared to other evolution algorithms. In [20] a hybrid algorithm of PSO and GA is introduced to solve the BSS problem. Since there's no guarantee that heuristics will result in an optimal solution, an exact optimization approach is used in this research. In [12] the authors represented their BSS problem as a mixed-integer linear programming (MILP) and solved it using an exact approach. Research effort has also been placed to solve large-scale optimization problems that accommodate nonlinearities. In [18] a generalized benders decomposition algorithm is used to solve the problem by dividing each sub-problem into multiple independent quadratic programming problems.

One of the approaches used for optimal scheduling is the rolling horizon predictive technique [21]-[23]. In [21] the rolling horizon mechanism is used for optimal control of an energy storage unit in a grid-connected microgrid. In [22] an online model predictive controller is demonstrated for a micro-grid with plug-in EVs. Also, Alison O'Connell [23] presented a rolling horizon optimization method that focuses on controlling the rate and times at which EVs charge. For the BSS models, the majority of research work preferred modeling the system as a day-ahead problem. In this regard, the model is based on EV appointments and the customers place their swapping requests a day in advance, thus, restricting the BSS scheduling. Whereas, the rolling horizon/window optimizer utilizes dynamic forecasting to forecast the swapping demand, therefore, it is more robust to uncertainties. In a real BSS system, this methodology is much better than offline approaches as it utilizes the predicted data to develop optimal dynamic scheduling. In this research, we employ a rolling horizon optimization (RHO) mechanism that establishes a dynamic optimization environment. Meanwhile, the RHO mechanism optimizes the system over shorter time intervals which reduces the computational time. The RHO is based on utilizing a forecasting engine to forecast data for a future time interval. The forecasted data such as the EVs swapping demand are updated on each roll/iteration during the scheduling interval. Various research efforts have been carried out towards forecasting the EV arrivals and their charging demand at EV charging stations. In terms of time series forecasting, there are several methods used for predicting future time intervals. In [24] and [25] the authors utilized the Autoregressive Integrated Moving Average (ARIMA) method as their forecasting engine. Also, time series forecasting using deep learning is one of these methods that could be used for predicting future time steps. Unlike backpropagation neural networks and convolutional neural networks, recurrent neural networks (RNN) are capable of taking a sequence of data and predicting a future sequence. RNNs has also the capability of updating the network state with the observed values instead of the predicted values [26] – [27].

The LSTM network is an evolution of the conventional RNN [28]. The empirical studies conducted in [28] show that time series forecasting using the LSTM outperforms the traditional ARIMA model. For example, The LSTM improves the average prediction accuracy by 85 % compared to the ARIMA method. Hence, we used the long-short term memory (LSTM) as our forecasting engine to forecast the EV battery swapping demand. While most of the BSS models in the literature assumed that the BSS provides this service for a single battery type, very few research work introduced battery heterogeneity into BSSs modeling. In [29] the authors assumed a heterogeneous battery stock with some impractical assumptions. For example, it was assumed that the customers submit a battery swapping request

TABLE I
A COMPARISON HIGHLIGHTING THE CHARACTERISTICS OF THIS RESEARCH

Features	BSS Operation Models in Previous Literature											BSS in this Research
	[16]	[6]	[13], [14], and [20]	[18]	[12] and [15]	[11]	[7]	[9]	[10]	[17]	[29]	
Battery Degradation	×	×	×	✓	✓	×	×	✓	✓	×	×	✓
Battery heterogeneity	×	×	×	×	×	×	×	×	×	×	✓	✓
Battery Charging Characteristics	✓	×	×	×	×	×	✓	✓	✓	×	×	✓
Charging Scheduling (G2B)	✓	✓	✓	✓	✓	✓	✓	✓	✓	✓	✓	✓
Discharging to grid (B2G)	✓	×	×	×	✓	✓	×	×	×	×	×	✓
Different Chargers	×	×	×	×	×	×	×	✓	×	×	×	✓
Multiple BSSs	×	✓	×	✓	×	×	×	×	×	✓	✓	×
Single BSS	✓	×	✓	×	✓	✓	✓	✓	✓	×	×	✓
Variable Charging Power	✓	×	×	✓	✓	×	×	×	✓	×	×	✓

and specify the battery type in advance. Hence, this system is not flexible and lacks dynamicity.

Based on the aforementioned discussion, it's clear that the BSS operations modeling is still in its primitive phase as more research about dynamic scheduling is required. Table I summarizes the characteristics of this research work concerning other literature works. As shown in Table I, this research integrates several features into the BSS operation at once compared to some other literature. From the table, it can be seen that most of the researchers considered a single battery type, whereas, few works only introduced multiple battery types. Therefore, we formulated a generalized model taking into account the battery heterogeneity.

In this paper, a new problem formulation for the dynamic operation of a BSS is proposed which makes it much closer to practical operation. Furthermore, a comprehensive study that compares the day-ahead operation, the rolling horizon dynamic operation, and the BSS unscheduled operation is presented. The main contributions of this research work are summarized as follows:

- The diversification of the arriving EV type is adopted in this model by introducing multiple units and sizes of batteries. Hence, the BSS can serve an EV requesting single or multiple battery units (e.g. electric buses, trucks, or even large size electric cars).
- To the best of the authors' knowledge, this is the first model that assesses the BSS optimization problem dynamically using an RHO mechanism while employing an LSTM recurrent neural network as a time series forecasting engine to predict the future EV's swapping demand.

The rest of the paper is organized as follows. A general description of the proposed BSS system is presented in section II. In section III, the mathematical formulation and the model details are explained. Demand forecasting and the RHO mechanism are illustrated in section IV. A set of case studies and the simulation output are presented in section V. Additionally, a detailed comparison between case studies and an analysis of the proposed approach are given in section VI. Finally, Section VII presents conclusions and future work.

II. The Structure of The Proposed BSS System

A general framework of the proposed BSS system is illustrated in Fig. 1. The BSS consists of five main parts, namely, i) The power system, ii) The charging partition, iii) The fully charged battery inventory (FCBI), iv) The swapping bays, and v) The BSS control center.

A. Details of the system model

In this paper, a fully automated swapping system using robots is proposed. Once a battery is fully charged it's automatically transferred to the FCBI. The BSS model is mainly providing service to EVs by unloading the DBs from the arriving EV and replacing it with a fully charged one from the FCBI. The BSS can also provide the service by swapping a partially charged battery directly from the charging racks. The minimum state of charge (SOC) of a partially charged battery

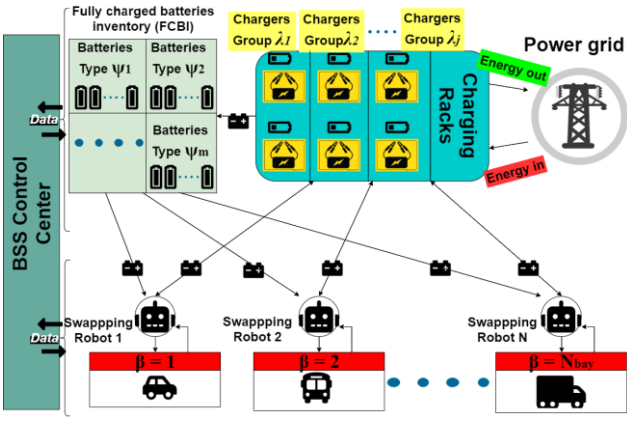

Fig. 1. The proposed BSS system structure.

cannot be less than a certain threshold ζ. The BSS has a number of swapping bays Nbay, each is defined with index β. Some bays are specified for EVs requesting a single battery unit, while some other bays are used to serve EVs requesting more than one battery unit (e.g. Electric busses or trucks). Meanwhile, the BSS has a heterogeneous battery stock that has different battery types ψ_m for serving different types of EVs. The types of EV batteries can vary due to the different manufacturers and models. To avoid problems such as compatibility which is one of the main concerns for lithium-ion batteries, the BSS has different groups of DC chargers λ_j. Each group of chargers are specified for a certain battery type and has the same rating. These chargers are advanced chargers that charge/discharge with a continuously controlled power to get more flexibility while supplying energy to the grid. Hence, the proposed BSS system fully utilizes the battery-to-grid (B2G), grid-to-battery (G2B), and battery-to-battery (B2B) concepts and efficiently provides grid ancillary services. Additionally, the BSS has a control center that is responsible for taking the optimal decisions of charging/discharging/swapping processes. Furthermore, the control center continuously monitors the BSS demand, the number of charged batteries in stock, the SOC of the batteries, and the price of electricity.

B. Assumptions

The following assumptions are made for the proposed BSS system:

- It is assumed that batteries are owned by the BSS so that it's responsible for their charging/discharging, state of health, and degradation.
- A heterogeneous battery inventory is proposed for serving different EV models from different manufacturers. Meanwhile, it's assumed that different EV types from the same manufacturer such as cars, buses, or trucks can use single or multiple units of a unified battery type.
- A fully automated swapping system is assumed with a proposed swapping service time under 10 minutes.

III. Optimization Model

In this section, an MINLP optimization model is formulated for the BSS optimal operations scheduling. The model is then linearized into a MILP to reduce the computational complexity.

A. The BSS mathematical model

The optimization model is given in (1)-(28) for batteries $b \in B = \{1,2,\dots,\mathrm{N}^{bat}\}$, swapping bays $\beta \in U = \{1,2,\dots,\mathrm{N}^{bay}\}$, chargers $c \in K = \{1,2,\dots,\mathrm{N}^{ch}\}$, type of batteries $\psi = \{\psi_1, \psi_2,\dots,\psi_m\}$, and a group of chargers $\lambda = \{\lambda_1, \lambda_2,\dots,\lambda_j\}$, where $[\psi_1 \cup \psi_2 \cup \dots \cup \psi_m = B]$, $[\psi_1 \cap \psi_2 \cap \dots \cap \psi_m = \{\phi\}]$, $[\lambda_1 \cup \lambda_2 \cup \dots \cup \lambda_j = K]$,$[\lambda_1 \cap \lambda_2 \cap \dots \cap \lambda_j = \{\phi\}]$; where m and j are the indices of battery types and chargers groups available at the BSS respectively. A group of chargers has chargers of the same type and characteristics. Each group of chargers is assigned to a certain battery type. In the following formulation chargers of group λ_j is assigned to the battery type ψ_m, where $(m = j)$. The number of chargers in each group λ_j is N_j^{ch}. In the objective function (1), the profit of the BSS is represented as the difference between the total revenue and the total costs. The total revenue of the BSS is represented as the revenue from the battery swapping to the customers R^s and the revenue from selling energy to the grid R^{B2G}. The costs in the system are mainly the cost of energy purchased from the grid to charge the batteries C^{G2B} and the battery degradation cost C^{DEG}.

$$\left.\begin{aligned} OBJECTIVE \rightarrow \max_{F}(O), \\ O = R^s + R^{B2G} - C^{G2B} - \mathrm{C}^{DEG} \end{aligned}\right\} \tag{1}$$

$$R^s = \left\{ \begin{aligned} &\sum_{(\tau\in T)}\sum_{(b\in B)}\sum_{(\beta\in U)} sw_{\tau,b,\beta} \times \mathrm{c}_b^{\mathrm{swap}} \\ &+ \sum_{(\tau\in T)}\sum_{(b\in B)} \frac{e^{max}{}_b}{100} \times \Delta soc_{\tau,b}^{swap} \times \mathrm{c}^{\mathrm{kWh}} \end{aligned} \right\} \tag{2}$$

$$R^{B2G} = \sum_{(\tau\in T)}\sum_{(b\in B)} \Delta\mathrm{t} \times \mathrm{c}_\tau^{\mathrm{gr}} \left(\eta^{\mathrm{dch}} \times p_{\tau,b}^{dch}\right) \tag{3}$$

$$C^{G2B} = \sum_{(\tau\in T)}\sum_{(b\in B)} \Delta\mathrm{t} \times \mathrm{c}_\tau^{\mathrm{gr}} \left(\frac{p_{\tau,b}^{ch}}{\eta^{\mathrm{ch}}}\right) \tag{4}$$

Subject to:

$$\Delta soc_{\tau,b}^{swap} = \sum_{(\beta\in U)} \left(soc_{\tau-1,b} - \mathrm{soc}_{\tau,\beta}^{\mathrm{ev}}\right) \times sw_{\tau,b,\beta} \quad \forall(\tau \neq 1) \in T, \forall\, b \in B, \tag{5}$$

$$\Delta soc_{\tau,b}^{swap} = \sum_{(\beta\in U)} \left(\mathrm{soc}_b^0 - \mathrm{soc}_{\tau,\beta}^{\mathrm{ev}}\right) \times sw_{\tau,b,\beta} \quad (\tau = 1) \in T, \forall\, b \in B, \tag{6}$$

$$ch_{\tau,b} + \sum_{(\beta\in U)} sw_{\tau,b,\beta} \leq 1 \quad \forall\tau \in T, \forall\, b \in B, \tag{7}$$

$$soc_{\tau,b} = soc_{\tau-1,b} + \frac{\left(p_{\tau,b}^{ch} - p_{\tau,b}^{dch}\right) \times \Delta\mathrm{t}}{\mathrm{e}_b^{\max}} \times 100\% - \Delta soc_{\tau,b}^{swap} \quad \forall(\tau \neq 1) \in T, \forall\, b \in B, \tag{8}$$

$$soc_{\tau,b} = \mathrm{soc}_b^0 + \frac{\left(p_{\tau,b}^{ch} - p_{\tau,b}^{dch}\right) \times \Delta\mathrm{t}}{\mathrm{e}_b^{\max}} \times 100\% - \Delta soc_{\tau,b}^{swap} \quad (\tau = 1) \in T, \forall\, b \in B, \tag{9}$$

$$(\mathrm{soc}_b^{max} - \mathrm{DOD}^{\max}) \leq soc_{\tau,b} \leq \mathrm{soc}_b^{max} \quad \forall\tau \in T, \forall\, b \in B, \tag{10}$$

$$soc_{\tau-1,b} \geq \zeta \times \sum_{(\beta\in U)} sw_{\tau,b,\beta} \quad \forall(\tau \neq 1) \in T, \forall\, b \in B, \tag{11}$$

$$\mathrm{soc}_b^0 \geq \zeta \times \sum_{(\beta\in U)} sw_{\tau,b,\beta} \quad (\tau = 1) \in T, \forall\, b \in B. \tag{12}$$

The decision variable vector $F = \left[p_{\tau,b}^{ch}, p_{\tau,b}^{dch}, ch_{\tau,b}, sw_{\tau,b,\beta}\right]^T$ includes the variables for batteries charging/discharging and swapping processes. In (2) the binary variable $sw_{\tau,b,\beta}$ represents the status of the battery b at any time τ and swapping bay β such that it's 1 if a battery is swapped and 0 otherwise. The pricing of the swapping service is divided into two parts: a) fixed price per replacement of a battery unit b) price per kWh exchanged with the customer. Therefore, the revenue from swapping R^s is achieved from the submission of two terms as shown in (2). In (3) and (4) the cost of energy charged from the grid and the income from energy discharged to the grid is calculated based on the electricity price. Equations (5) and (6) calculate the drop in the SOC of a certain battery b if it's replaced by a DB of an EV arriving with $\mathrm{soc}_{\tau,\beta}^{\mathrm{ev}}$ at any time τ. If a battery b is not swapped at any swapping bay β at time τ, therefore, the values of the variables $sw_{\tau,b,\beta}$ and $\Delta soc_{\tau,b}^{swap}$ are 0. Constraint (7) ensures that any battery at any time τ is either swapped at any swapping bay β if $sw_{\tau,b,\beta}$ is 1 or charging at the charging racks if the binary variable $ch_{t,b}$ is 1. Thus, both charging and swapping processes cannot occur at the same time for the same battery. Furthermore, a certain battery b cannot be replaced at two different swapping bays at the same time slot as there is a submission on the β index as shown in (7). The batteries are stored at the FCBI if the binary variables $sw_{\tau,b,\beta}$ and $ch_{t,b}$ are both zeroes and if its SOC is 100%.

In (8) and (9) the SOC of each battery b at any time τ is calculated while considering the SOC at the end of the previous time slot $\tau - 1$ and the charging & discharging power efficiencies η^{ch} & η^{dch}. As shown in (10), the SOC of any battery in the BSS cannot be discharged more than the maximum depth of discharge DOD^{max}. Also, the SOC cannot exceed $\mathrm{soc}_b^{max} = 100\%$. The proposed BSS model provides the option for swapping partially charged batteries from the charging racks. Equation (11) is used to satisfy the option of flexible SOC by serving partially charged batteries to customers. In (11), any battery at the BSS is eligible for swapping if it maintains a SOC equal to or above a certain threshold ζ. As a result, if a customer arrives with a DB at a time τ, the SOC of the served charged battery at the end of time slot $\tau - 1$ has to be above the threshold ζ. Similarly, equation (12) ensures that the initial soc_b^0 for any battery at the BSS at the beginning of the day is above the threshold ζ if this battery is to be swapped at the first time slot ($\tau = 1$).

The BSS model also offers serving multiple batteries for EVs requesting more than one battery unit as in (13) and (14):

$$\sum_{(b\in B)} sw_{\tau,b,\beta} = \mathrm{N}_{\tau,\beta}^{\mathrm{units}} \times M_{\tau,\beta} \quad \forall t \in T_\beta^{arv}, \forall\, \beta \in U, \tag{13}$$

$$sw_{t,b,\beta} = 0 \quad \forall\tau \in T_\beta^{arv'}, \forall\, b \in B, \forall\, \beta \in U, \tag{14}$$

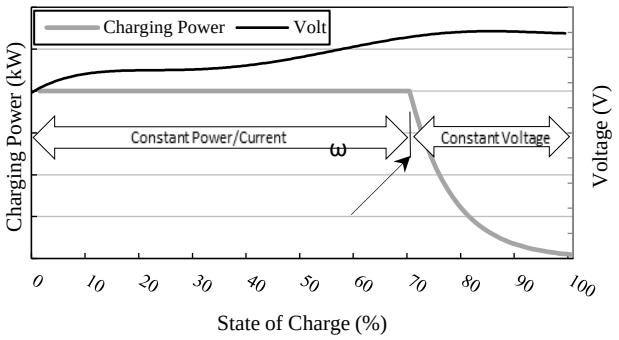

Fig. 2. Charging characteristics of a Li-ion battery cell.

where $\left[T_\beta^{arv} \cup T_\beta^{arv'} = T\right]; \left[T_\beta^{arv} \cap T_\beta^{arv'} = \{\phi\}\right]$.

At any time slot τ only one customer can swap single or multiple battery units at the same bay β. Constraint (13) states that EVs arriving at bay β and time τ requesting $\mathrm{N}_{\tau,\beta}^{units}$ units of batteries for swapping could be served or not; where $M_{\tau,\beta}$ is a binary variable equal to 1 if the EV is served and 0 otherwise. Equation (14) sets the variable $sw_{\tau,b,\beta}$ to zero at the time slots without any arrivals $T_\beta^{arv'}$ at bay β.

In (15) and (16), the total number of EVs served and batteries swapped are calculated respectively as follows:

$$\mathcal{N}^{served} = \sum_{(\tau \in T)} \sum_{(\beta \in U)} \frac{\sum_{b \in B} sw_{\tau,b,\beta}}{\mathrm{N}_{\tau,\beta}^{units}} \qquad \forall \mathrm{N}_{\tau,\beta}^{units} \neq 0, \tag{15}$$

$$\mathcal{N}^{BAT-SW} = \sum_{(\tau \in T)} \sum_{(\beta \in U)} \sum_{(b \in B)} sw_{\tau,b,\beta} \tag{16}$$

The net power flow at the BSS P_τ^{net-TF} should not exceed the transformer rated power P^{MAX-TF} as shown in (17). P_τ^{net-TF} is calculated at any time τ as the difference between the total charged and discharged power from all the batteries as defined in (18).

$$-\mathrm{P}^{MAX-TF} \leq P_\tau^{net-TF} \leq \mathrm{P}^{MAX-TF} \qquad \forall \tau \in T, \tag{17}$$

$$P_\tau^{net-TF} = \sum_{(b \in B)} p_{\tau,b}^{ch} - p_{\tau,b}^{dch} \qquad \forall \tau \in T. \tag{18}$$

B. Charging Characteristics Modeling

To fully utilize the benefits from the grid services, variable-rate chargers for charging Lithium-ion (Li-ion) batteries are considered in this model. Furthermore, the charging characteristics of Li-ion batteries are considered for the model to be close to practical operation. The typical charging characteristics of a Li-ion battery cell are shown in Fig. 2. As shown in the figure, the charging starts with a constant power until the SOC reaches a certain percentage ω % before it decreases exponentially [9]. This is known as a constant-current/constant-voltage charging strategy [9]. In this model, continuously controlled variable chargers are used. Thus, a combination between the variable charging and the constant-current/constant-voltage charging strategy is implemented. In our proposed BSS model, the charging power curve in Fig. 2 is considered as the upper limit for charging. The combination of (19) and (20) models the charging characteristics for li-ion batteries as they define the bounds on the charging power. The charging characteristics are modeled as a function of the battery SOC as it decreases exponentially less than p_c^{MAXc} when the SOC exceeds a certain ω% as shown in (19). In (21) the power discharged from any battery should be less than the upper limit p_c^{MAXd}. The parameters p_c^{MAXc} and p_c^{MAXd} are set according to the group of chargers λ_j assigned to each battery type ψ_m; recall, in this model, we assign $(m = j)$.

$$0 \leq p_{\tau,b}^{ch} \leq \left(\mathrm{p}_c^{MAXc} \times e^{\frac{\omega - soc_{t,b}}{\mathrm{P}_c^{\mathrm{MAXc}}}}\right) \times ch_{\tau,b} \qquad \forall \tau \in T \ \forall b \in \psi_m \ \forall c \in \lambda_j \ \forall (m = j) \in \psi, \tag{19}$$

$$0 \leq p_{\tau,b}^{ch} \leq \mathrm{p}_c^{MAXc} \times ch_{\tau,b} \qquad \forall \tau \in T \ \forall b \in \psi_m \ \forall c \in \lambda_j \ \forall (m = j) \in \psi, \tag{20}$$

$$0 \leq p_{\tau,b}^{dch} \leq \mathrm{p}_c^{MAXd} \times ch_{\tau,b} \qquad \forall \tau \in T \ \forall b \in \psi_m \ \forall c \in \lambda_j \ \forall (m = j) \in \psi, \tag{21}$$

C. Battery Heterogeneity

Unlike most of the BSS models that consider a single battery type, the proposed BSS framework introduces battery heterogeneity to provide a realistic model for the BSS operation. Thus, multiple battery capacities are considered in the optimization framework in order to unify battery management and achieve global gains.

In (22) the subset $T'_{m,\beta}$ represents the time slots at which no EV arrivals are requesting a battery of type ψ_m at any swapping bay β. Batteries at the BSS of type ψ_m can't be swapped at $T'_{m,\beta}$ by setting $sw_{\tau,b,\beta} = 0$ at these time slots. Due to the different types of batteries available, each type ψ_m is assigned for a group of chargers λ_j, where $(m = j)$. In (23) the total number of batteries of a certain type ψ_m that can be charged at the same time are restricted to the number of chargers N_j^{ch} in group λ_j assigned to this type

$$sw_{\tau,b,\beta} = 0 \qquad \forall \tau \in T'_{m,\beta} \ \forall b \in \psi_m \ \forall m \in \psi \ \forall \beta \in U, \tag{22}$$

$$\sum_{(b \in \psi_m)} ch_{\tau,b} \leq \mathrm{N}_j^{\mathrm{ch}} \qquad \forall \tau \in T \ \forall (m = j) \in \psi, \tag{23}$$

where $(T'_{m,\beta} \subset T)$ for the time slots at which there are no EV arrivals requesting type *m* batteries at bay β.

D. Battery Degradation Effect

The batteries in the BSS undergo many charging/discharging cycles which reduce the battery lifetime and result in decreasing the maximum capacity of the battery. In this research paper, the battery characteristics are highly dependent on the number of cycles, as illustrated in [30], whereas, other battery chemistries are highly sensitive to the DOD^{max} [31]. The degradation in a certain battery SOC is calculated as a function of the number of cycles as shown in Appendix A.

In the BSS operation model, it's very likely for any battery at the BSS to suffer a negligible degradation in its SOC in just one day. So, the battery degradation effect is more significant in the BSS planning problems. However, the degradation in the battery SOC is considered in this model to achieve a more realistic profit. In the BSS operation model, the total daily battery degradation cost C^{DEG} is the minimum cost in the system. Also, its variation is minor with the charging scheduling in daily operation models. Hence, for simplicity, the

battery degradation cost is calculated for the obtained number of cycles after solving the optimization model. Furthermore, embedding its calculations within the optimization model will not result in a much-enhanced solution and it would rather increase the model nonlinearity.

E. Model Linearization

To decrease the computational complexity, some constraints are linearized. Equation (5) performs the multiplication of a positive variable and a binary variable $soc_{\tau-1,b} \times sw_{\tau,b,\beta}$ which is linearized as shown in (24)-(27). The nonlinear term in (5) is replaced by a positive variable $z_{t,b,\beta}$ which equals to $soc_{\tau-1,b}$ from (26) and (27), if $sw_{\tau,b,\beta} = 1$. Whereas, if $sw_{\tau,b,\beta} = 0$, the variable $z_{\tau,b,\beta}$ is forced to 0 from (25) and (26) since it's a positive variable.

Equation (19) is linearized by (28) which is a linear fitting for the exponential term, where α and γ are the coefficients of the linear fit, and these coefficients change based on the charger rating and characteristics. The effect of linearization is further tested on one of the case studies that are presented later in section V.

$$\Delta soc_{\tau,b}^{swap} = \sum_{(\beta \in U)} \left(z_{\tau,b,\beta} - \mathrm{soc}_{\tau,\beta}^{\mathrm{ev}} \times sw_{\tau,b,\beta}\right) \quad \forall(\tau \neq 1) \in T, \forall\, b \in B, \tag{24}$$

$$z_{\tau,b,\beta} \leq sw_{\tau,b,\beta} \times \mathrm{soc}_b^{max} \quad \forall \tau \in T_\beta^{arr}, \forall\, b \in B, \forall\, \beta \in U, \tag{25}$$

$$z_{\tau,b,\beta} \geq soc_{\tau-1,b} - (1 - sw_{\tau,b,\beta}) \times \mathrm{soc}_b^{max} \quad \forall(\tau \neq 1) \in T, \forall\, b \in B, \forall\, \beta \in U, \tag{26}$$

$$z_{\tau,b,\beta} \leq soc_{\tau-1,b} \quad \forall(\tau \neq 1) \in T, \forall\, b \in B, \forall\, \beta \in U, \tag{27}$$

$$p_{\tau,b}^{C} \leq -\alpha soc_{\tau,b} + \gamma \quad \forall \tau \in T, \forall b \in B. \tag{28}$$

IV. Rolling Horizon Predictive Scheduling

The idea of rolling horizon optimization is to consider forecasted data over a limited horizon in addition to the currently available information to develop optimal decisions. The rolling horizon mechanism can be implemented by defining three horizons—namely, the scheduling horizon (T), the control horizon ($\boldsymbol{C}$), and the forecasting horizon ($\boldsymbol{u}$) [32]. For a BSS, at each time slot τ, the optimization model considers the current EV arrivals at the control horizon and the forecasted arrivals at future time slots $\tau + \boldsymbol{u}$ over the scheduling period T as presented in Fig. 3 where $1 \leq \boldsymbol{u} \leq N_T - 1$; N_T is the number of time slots in the scheduling horizon.

A. LSTM Forecasting Engine

In the proposed operation mechanism, a forecasting engine is required to forecast the swapping demand for future time slots. The forecasting is mainly done based on the historical data of the EV arrivals. To forecast the number of EV arrivals at each time slot through the day, RNNs is an efficient time series forecasting engine that allows feeding values forward in time since it uses not only the input data but also the previous outputs for making the current prediction. However, it's very hard to train and forgettable so we used an evolution of the RNN which was introduced by Hochreiter and Schmidhuber [33]. This network has a gated memory unit for neural networks and it is capable of learning long-term dependencies and remembering

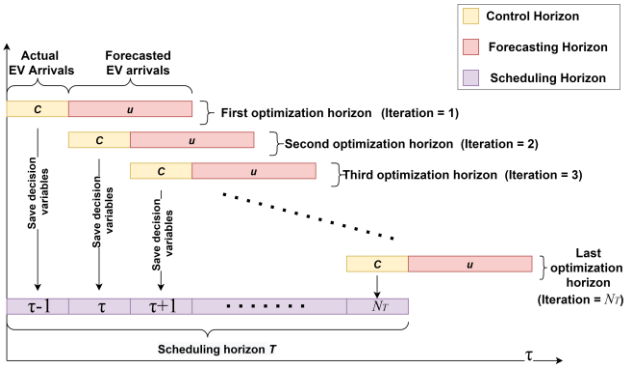

Fig. 3. The rolling horizon optimization mechanism

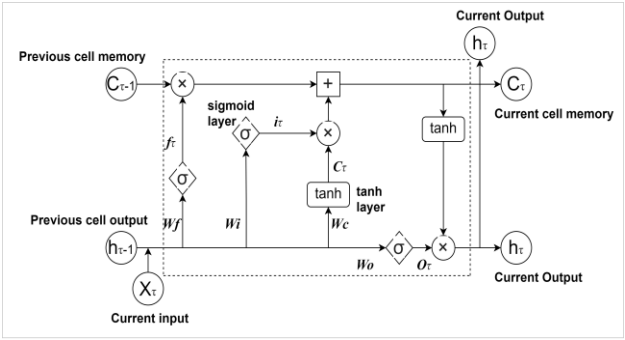

Fig. 4. The structure of the LSTM cell.

information for long periods of time. Fig. 4 shows the LSTM repeating module at time τ.

The LSTM network has memory blocks called cells and 3 gates managing the memory contents, each gate is a logistic function with weighted sums. Equations (29), (30), and (31) represent the forget gate, input gate, and output gate of each memory block at time τ respectively. The sigmoid function in each decides about the data that will be omitted from each cell. For a memory block, with J number of memory cells and an input activation vector of $X_\tau \in R^I$, the output activation vector is $O_\tau \in R^J$, and the current state vector is $C_\tau \in R^J$.

The input gate decides which new inputs flow into the cell state. The forget gate determines which values from the old output to forget and which values remain by looking at the current input (X_τ) and the previous output ($h_{\tau-1}$). Whereas, the output gate decides about values to be executed and it's determined by utilizing the state vector from the previous step $C_{\tau-1}$. An intermediate state vector $\widehat{C_\tau} \in R^J$ is calculated in (32) and considered as a candidate state vector. Equation (33) is responsible for updating the current cell state which is equal to the values omitted from the previous cell state plus the new candidate values entering the cell state. The LSTM performance is evaluated using the root mean square error (RMSE) as in [26]. The output values from the output gate are enhanced and produced in a filtered version $h_\tau \in R^J$ as shown in (34).

$$f_\tau = \sigma\left(W_f \times + U_f \times h_{\tau-1} + b_f\right) \tag{29}$$

$$i_\tau = \sigma(W_i \times X_\tau + U_i \times h_{\tau-1} + b_i) \tag{30}$$

$$O_\tau = \sigma(W_o \times X_\tau + U_o \times h_{\tau-1} + b_o) \tag{31}$$

$$\widehat{C_\tau} = tanh(W_c \times X_\tau + U_c \times h_{\tau-1} + b_c) \tag{32}$$

$$C_\tau = f_\tau \otimes C_{\tau-1} + i_\tau \otimes \widehat{C_\tau} \tag{33}$$

$$h_\tau = O_\tau \otimes tanh(C_\tau) \quad (34)$$

where b_f, b_i, b_o and b_c are the corresponding bias of f_τ, i_τ, O_τ, and $\widehat{C_\tau}$ respectively. W_f, W_i, W_o, and W_c represent the corresponding input weight matrices having $(J \times I)$ dimensions. Whereas U_f, U_i, U_o, and U_c are matrices with dimensions $(J \times J)$ and represent the recurrent connections. The sign $\otimes$ is used as an indication for element-wise multiplication. The sigmoid function (σ) and the hyperbolic tangent function are defined in (35) and (36) as follows:

$$\sigma(\boldsymbol{Z}) = \frac{1}{1+e^{-\boldsymbol{Z}}} \quad (35)$$

$$\tanh(\boldsymbol{Z}) = \frac{e^{\boldsymbol{Z}} - e^{-\boldsymbol{Z}}}{e^{\boldsymbol{Z}} + e^{-\boldsymbol{Z}}} \quad (36)$$

B. Proposed BSS Dynamic Scheduling Mechanism

The framework combining the LSTM and the RHO is further detailed in lines 1-13 in Algorithm 1 and in Fig. 5 as well. The algorithm starts by taking the historical data of the EV arrivals as an input; then it initializes the length of the control horizon, forecasting horizon, and scheduling horizon. The control horizon contains the current EV arrivals at the BSS, whereas, the forecasting horizon contains the predicted arrivals. The LSTM forecasting engine utilizes the historical arrivals data to predict future time slots as shown in lines 4-10 in algorithm 1. The algorithm then uses a certain solver to solve the optimization problem over the interval $\boldsymbol{C} + \boldsymbol{u}$ as shown in the flow chart in Fig. 5.

Finally, the values of the control horizon variables are saved, and a new iteration starts while updating the historical data with the actual arrivals in $\boldsymbol{C}$. The optimization horizon keeps rolling until the scheduling horizon is completed and the program terminates. To establish the dynamic scheduling mechanism, optimization and forecasting are implemented in two interdependent software programs. As shown in Fig. 5, the RHO framework is implemented in MATLAB, whereas, each optimization iteration in Fig. 3 is solved using GAMS [34].

Algorithm. 1: Pseudocode for the LSTM-based RHO

Input: Historical EV arrivals data and current EV arrivals
Output: RHO scheduling for the BSS operations
Initialize $\boldsymbol{C}$, $\boldsymbol{u}$, N_T, and the length of the training set (Q)
1: **for** τ = 1: ($N_T - 1$) **do**
2: Update the system state with the EV arrivals N_τ^{arr} in $\boldsymbol{C}$
3: LSTM Forecasting for the interval $\tau + \boldsymbol{u}$:
4: Data preprocessing (e.g. normalize the training set)
5: Create the input sequence and train LSTM:
6: X^T={$X_{\tau-Q}, \cdots, X_{\tau-2}, X_{\tau-1}$}={$N_{\tau-Q}^{arr}, \cdots, N_{\tau-2}^{arr}, N_{\tau-1}^{arr}$}
7: Predict output sequence O ⟵LSTM(X):
8: O^T = {$N_\tau^{arr}, N_{\tau+1}^{arr}, \cdots, N_{\tau+\boldsymbol{u}}^{arr}$} = {$O_\tau, O_{\tau+1} \cdots, O_{\tau+\boldsymbol{u}}$}
9: Evaluate the forecasting performance using RMSE
10: Update the training interval $Q \coloneqq Q + \boldsymbol{C}$
11: Run BSS scheduling model over the horizon $\boldsymbol{C} + \boldsymbol{u}$
12: Save the decision variables F for the period $\boldsymbol{C}$
13:**end for**

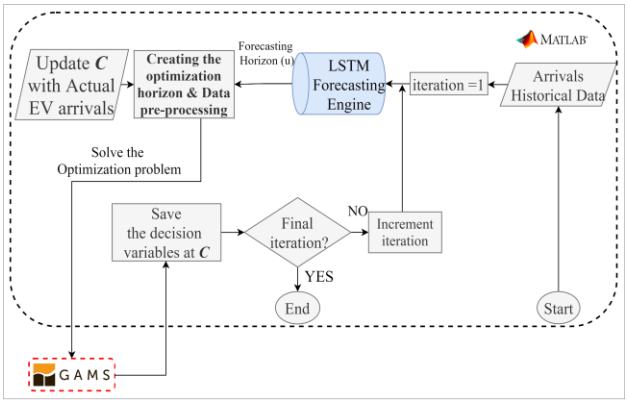

Fig. 5. Proposed LSTM-based RHO algorithm structure.

V. Case Studies and Simulation

This section carries out a set of case studies that show the effectiveness of the proposed dynamic scheduling mechanism. The cases presented in this study are mainly: the BSS unscheduled operation, day-ahead scheduling, and RHO scheduling. In all cases, the simulation is applied to a BSS serving two types of batteries with ratings of 16 kWh and 42 kWh. Additionally, two types of chargers are available at the BSS with ratings of 8 kW and 25 kW. The model is defined as a MILP; it is implemented in GAMS 30.3.0 and solved using the commercial mixed-integer linear solver CPLEX [34]. The LSTM network is trained and implemented using MATLAB [35]. The swapping service is provided within 10 minutes, thus the simulation is tested over 144-time slots equivalent to the 24 hours of the day. Table II defines the parameters used in the simulation. The parameters are mainly the prices of the swapping services, the operation costs, limitations on charging/discharging, and limitations on the power exchange with the power grid. The actual EV arrivals and the electricity

TABLE II
Parameters of the BSS Simulation

Parameters	Value
$b \in \psi_1$ indices	$b = [1-30]$
$b \in \psi_2$ indices	$b = [31-60]$
c_b^{swap}	500 ¢ $\forall b \in \psi_1$, 1200 ¢ $\forall b \in \psi_2$
c^{kWh}	50 ¢/kWh
DOD^{max}	80%
e_b^{max}	16 kWh $\forall b \in \psi_1$, 42 kWh $\forall b \in \psi_2$
ω	70%
N^{ch}	26; $N_1^{ch} = N_2^{ch}$=13
No. of batteries (N^{batt})	60; 30 of type ψ_1+ 30 of type ψ_2
No. of bays (N^{bay})	3
No. of EV arrivals	150
p_c^{MAXc}, p_c^{MAXd}	8 kW $\forall c \in \lambda_1$, 25 kW $\forall c \in \lambda_2$.
Batteries of type ψ_1	Charged with chargers group $c \in \lambda_1$
Batteries of type ψ_2	Charged with chargers group $c \in \lambda_2$
P_{ch}^{grid}, P_{dch}^{grid}	429 kW
soc_b^0	100 %
ζ	90 %
Δt	1/6
η^{ch}, η^{dch}	0.94
μ_b^{deg}	4200 ¢ $\forall b \in \psi_1$, 1600 ¢ $\forall b \in \psi_2$

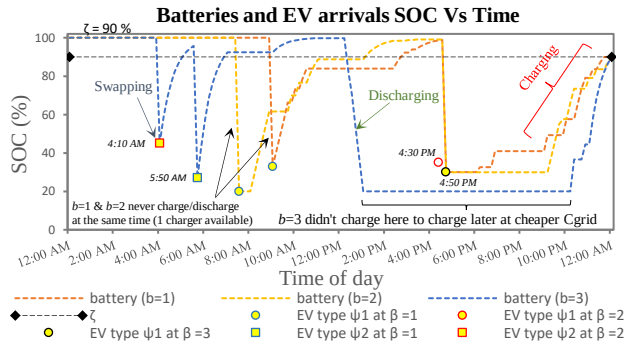

Fig. 6. Day-ahead scheduling for a small battery inventory

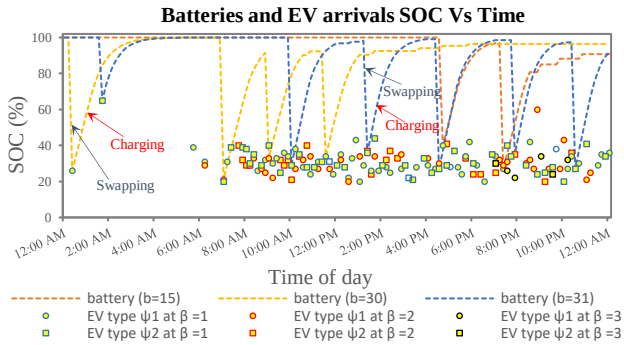

Fig. 7. (a) The SOC and the type of EVs arrivals, and (b) the SOC of a sample of three batteries in the unscheduled operation case of BSS.

price (Cgrid) are presented in Fig. 8 and Fig. 11, respectively. In figures (3-5, and 8) an EV requesting a type ψ_m battery at the β^{th} bay is denoted by EV type ψ_m at β.

A. *Day-Ahead Scheduling for a Small Battery Inventory.*

This is an illustrative case study with few batteries and EVs that validates the optimization model and ensures meeting the constraints in section III. The same values of the parameters from Table II are used. However, for simplicity, the number of batteries is reduced to three units: two of type ψ_1 and one type ψ_2. Also, only 1 charger is available for each battery type. Six customers arrived at different swapping bays and different time slots of the day. In all case studies presented in this section, EVs requesting more than one battery unit are marked in black on the figures and arrive at the third bay ($\beta = 3$). In Fig. 6, batteries with indices ($b = 1\,\&\,2$) are of type ψ_1, whereas batteries with index ($b = 3$) are of type ψ_2. Day-ahead scheduling is applied on the assumed EV arrivals in Fig. 6. For day-ahead scheduling, it should be assumed that batteries have the same SOC conditions at the beginning and at the end of the day. However, most of the literature work using the day-ahead model disregarded charging the batteries at the end of the day as in [12]. Hence, all the batteries are depleted, thus, achieving a high profit but the next day will start with a different initial SOC for the batteries. Hence, in the day-ahead case, it is assumed that the day starts and ends with charged batteries having a SOC greater than or equal to 90%. Therefore constraint (37) is added for charging the batteries at the end of the day at $\tau = 144$ to SOC 90% or above. Thus, ensuring batteries are charged before the beginning of the next day.

$$soc_{\tau=144,b} \geq 90\% \qquad \forall\, b \in B. \qquad (37)$$

In Fig. 6, the sudden drop in a certain battery SOC indicates swapping this battery with the depleted one of the arriving EV. In all case studies, the EV arrivals highlighted in yellow represent served customers. EVs arriving at 4:10 AM and 5:50 AM request type ψ_2 batteries and it can be seen that only batteries with index ($b = 3$) swapped. Whereas, the rest of EVs arrivals request type ψ_1 batteries and could only be swapped with batteries ($b = 1$) or ($b = 2$).

It can be observed that the SOC of batteries swapped at any time τ is greater than or equal to the threshold ($\zeta = 90\%$) at the end of the previous time slot $\tau - 1$ before swapping. Since there's only one charger available for type ψ_1 batteries, therefore ($b = 1$) and ($b = 2$) cannot be charging at the same time; one is charging while the other is constant and vice-versa. The large EV arriving at 4:50 PM requests 2 battery units of type ψ_1, thus the optimization solver favored swapping 2 units to this customer and rejected the customer requesting one unit at 4:30 PM. A total profit of $71.73 is obtained for this simple illustrative case while using the linearized constraints (24) – (28). Whereas, a total profit of $70.76 is obtained without linearization, which is 1.35 % lesser. Hence, the linearization effect is very minor and it doesn't sacrifice any of the system functionalities. In the non-linearized case, a global optimization solver is employed to solve the proposed MINLP using a branch-and-reduce optimization navigator (BARON) solver 19.12.7 [34]. Using this solver to solve the non-linearized version of the case studies presented in the following subsections is computationally expensive.

B. *Unscheduled Operation with a Greedy Algorithm (case 1)*

This case study represents the base case for a BSS operating without optimization. The idea is mainly based on serving a customer by swapping his DB with a charged one if available, otherwise, batteries are either charging or stored at the FCBI. Hence, the batteries, in this case, are charged as soon as possible and discharging to the grid is excluded. The algorithm used in this case is considered as a greedy algorithm as it tends to serve more customers by charging DBs immediately after the swapping process as shown in Fig. 7. Meanwhile, the discharging to the power grid is disabled in order to keep batteries charged to serve more customers. The greedy algorithm used in this case is presented in Appendix B.

The parameters in Table II are used in this case study. Fig. 7 shows the SOC for a sample of three batteries during the day. For comparison, the EV arrivals used in this case are the same actual EV arrivals in cases 2 and 3. In Fig. 7, it can be seen that the batteries are charging as soon as possible to serve more customers while disabling the discharge option. The hourly profit, in this case, is presented in Fig. 8, the profit in red is a negative profit due to replenishing the energy of the two DBs received from the two customers arriving at the beginning of the day. Meanwhile, there are no EV arrivals at these time slots to achieve revenue from swapping. This operation resulted in a total daily profit of $1963.8, 150 customers were served, and 162 batteries were swapped.

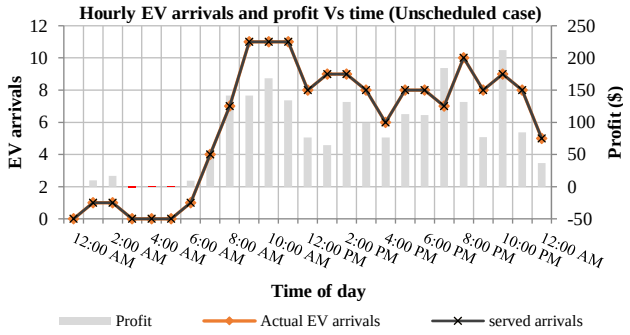

Fig. 8. The profit and the number of EV arrivals at each hour in the unscheduled operation case study.

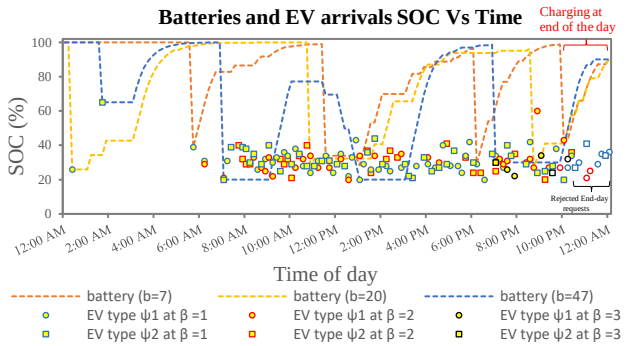

Fig. 9. (a) The SOC and the type of EVs arrivals, and (b) the SOC of a sample of three batteries in the day-ahead operation of the BSS.

C. *Day-ahead Scheduling with EV Appointments (case 2)*

In this case study, day-ahead scheduling is applied on the same actual EV arrivals data in the unscheduled operation and the rolling horizon scheduling cases. In the day-ahead mode of operation, these EV arrivals are considered as swapping requests placed in advance. Thus, each customer reserves an appointment for swapping at a specific time. The day-ahead optimization simulation is applied to the 144-time slots of the day and an optimal profit that maximizes the daily profit was obtained. Fig. 9 shows the SOC for a sample of three batteries during the day. The simulation starts with fully charged batteries. It's clear from Fig. 9 and Fig. 10 that the customers arriving at the end of the day will not be served since all batteries are charging to achieve a SOC above 90% at the end of the day according to (37). The high energy consumed at the end of the day to charge all the depleted batteries before the next day resulted in a negative profit at the last two hours as shown in Fig. 10. The day ahead scheduling resulted in a total daily profit of $1792.5 while serving 136 customers and swapping 142 battery units. In Fig. 11, the total B2G, G2B, and B2B power of the BSS at any time during the day is represented. Additionally, it can be observed that more energy is sold to the grid at the highest electricity price.

An extended version of the day-ahead case is capable of achieving a higher profit by eliminating the constraint (37). This solution doesn't account for keeping the batteries charged before the beginning of the next day. In this case, it should be assumed that the BSS receives newly charged batteries at the beginning of the next day that were previously charged elsewhere. Thus, the solution, in this case, is considered as an ideal solution as it utilizes the actual information of the swapping demand and the electricity price for the whole day. Although this case is impractical, it results in a total profit of $2289.76 which is the highest possible profit that could be achieved by the proposed BSS model.

D. *Rolling Horizon Scheduling (case 3)*

This case study assesses the BSS dynamic scheduling using a rolling horizon optimization environment. The scheduling horizon is 24 hours of the day. The control horizon is the 10 minutes one-time slot that has the actual EV arrivals, whereas a forecasting horizon of 6 hours is used. Forecasting is carried out for each battery type independently. This Model utilizes historical data of EV arrivals in an EV parking lot in Toronto,

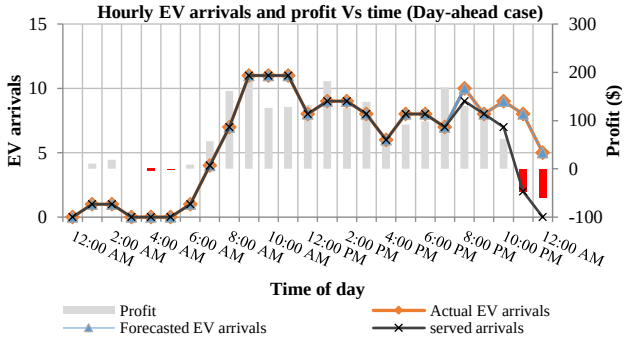

Fig. 10. The profit and the number of EV arrivals at each hour in the day-ahead operation case study.

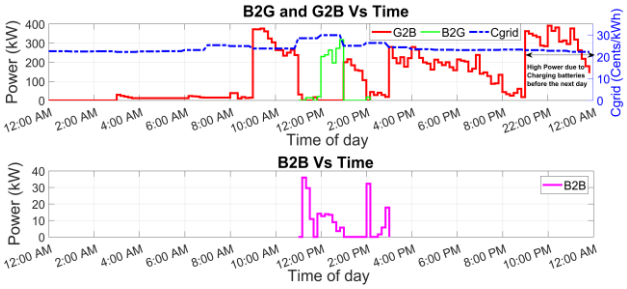

Fig. 11. Total energy charged/discharged from the power grid and battery to battery energy exchange in the day-ahead operation case study.

Ontario, Canada. These data are obtained from Toronto parking authority. In Fig. 12, the LSTM network utilizes the historical data of four consecutive days of the EV arrivals requesting battery type ψ_1 to forecast future arrivals. The historical data of the EV arrivals were recorded every 10 minutes. The LSTM network state is continuously updated with the actual EV arrivals in the control horizon to update the forecasting horizon as illustrated previously in section IV. For comparison, the actual EV arrivals data are the same data used in cases 1 and 2.

The RHO simulation is applied to 37-time slots on each roll/iteration. Each single time slot represents the 10 minutes control horizon, whereas 36-time slots represent a 6 hours forecasting horizon. A total number of 144 optimization iterations are performed using the RHO algorithm for a complete day. The RHO runs continuously since the time horizon keeps rolling while forecasting new arrivals and ensuring that the swapping conditions are met. As a result, the proposed RHO mechanism doesn't need to force batteries to be charged at the end of the day such as in the day-ahead model.

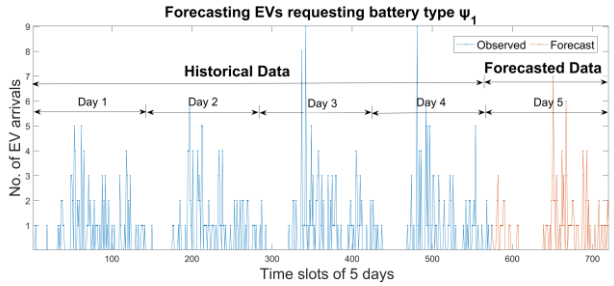

Fig. 12. Forecasting for the EV arrivals requesting a certain type of battery.

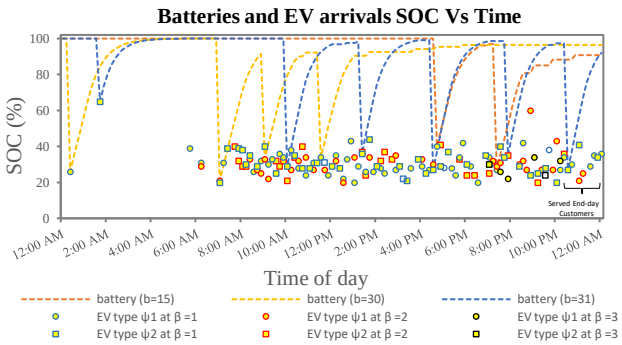

Fig. 13. (a) The SOC and the type of EVs arrivals, and (b) the SOC of a sample of three batteries in the rolling horizon scheduling case of BSS.

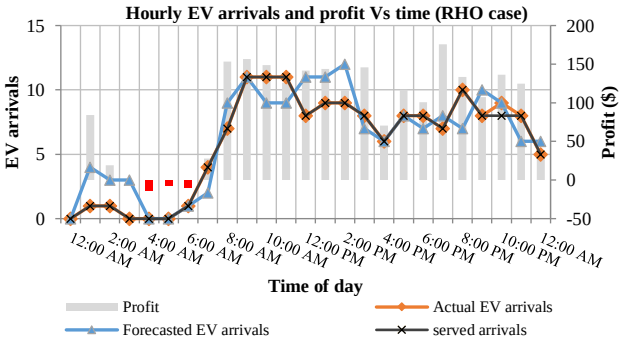

Fig. 14. The profit and the number of EV arrivals at each hour in the rolling horizon operation case study.

The day-ahead model is less flexible and lacks dynamicity since it's based on appointments. Unlike day-ahead operation, the RHO provides a dynamic scheduling environment that is robust to uncertainty. Additionally, RHO iterations continue scheduling for the new day after the day ends while always ensuring the SOC of the charged batteries is above 90% prior to swapping according to (11) in section III. Hence, RHO serves end-day customers as shown in Fig. 13 and Fig. 14.

As shown in Fig. 15, The B2G discharge at the beginning of the day took place since the forecasting horizon initially contained few arrivals during the first few iterations. Hence, it results in a high revenue from discharging. As the window rolls, more customers appear on the forecasting horizon and the batteries are charged in advance in order to serve the forecasted customers. This is also reflected in Fig. 14 as a high profit at the beginning of the day followed by a negative profit due to charging the batteries when the customers showed up in the forecasting horizon. The RHO served 149 customers by swapping 158 battery units and resulted in a total daily profit of

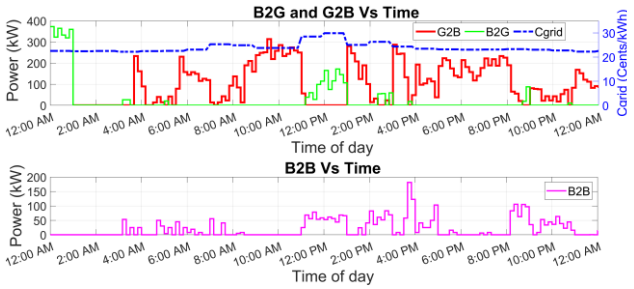

Fig. 15. Total energy charged/discharged from the power grid and battery to battery energy exchange in the RHO operation case study.

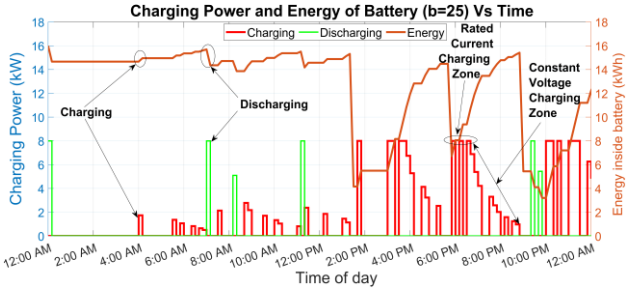

Fig. 16. The charging power and energy are stored inside batteries with an index (b=25).

$2128.1 which is more than the previous cases.

In Fig. 16, the charging characteristics of one of the batteries at the BSS are illustrated. The figure presents the plot of the energy and the charging power of a battery of type ψ_1 with index ($b = 25$). It can be seen that the battery is charged with a value less than or equal to the maximum charging limit until its SOC reaches 70%. When the SOC threshold ω exceeds 70 % there's a kind of exponential decrease from the maximum charging rate in the constant voltage charging mode. This proves that the results satisfy the constraints governing the charging characteristics of Li-ion batteries.

VI. Results and Analysis

In this section, a detailed comparison between the results of different case studies is presented. Additionally, an analysis has been conducted for the proposed RHO approach that shows the effect of using different forecasting intervals on the system. The numerical results used in this section verify the efficacy of the proposed approach and show how it outperforms other existing approaches. Finally, we concluded our analysis with some policy implications that were proposed based on the obtained results.

A. Comparison between Different Case Studies

In this subsection, a comparison between the obtained results of the three previous case studies is presented in Table III and Fig. 17. As shown in Table III, RHO scheduling (case 3) resulted in the highest profit, whereas the day-ahead scheduling (case 2) has the lowest profit. It can be also seen that the revenue from swapping in the unscheduled operation (case 1) has the highest value due to its greedy algorithm that tends to serve more customers.

For all the cases, it can be noticed that the charging of the batteries has the highest cost C^{G2B} as it represents 86% - 88% of the total cost. The cost of energy in case 1 is 804.52 $/day,

TABLE III
OPTIMIZATION OUTPUT COMPARISON BETWEEN DIFFERENT CASE STUDIES

Output	Unscheduled Operation	Day-ahead Operation	RHO Operation	Unit
O	1963.8	1792.5	2127.5	$/day
R^S	2877	2311	2491	$/day
R^{B2G}	0	283	461	$/day
C^{G2B}	804.52	704	717	$/day
C^{DEG}	108.7	97.4	107.5	$/day
$\mathcal{N}^{served}$	150	136	149	Unit
$\mathcal{N}^{BAT-SW}$	162	142	158	Unit

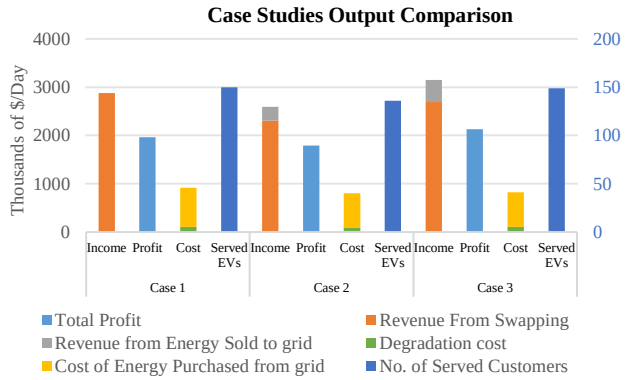

Fig. 17. Comparison between the outputs of different case studies.

which is higher than the other cases due to charging the DBs as soon as possible. Whereas, the day-ahead model has the lowest charging cost of 704 $/day as it observes the electricity price for the whole day, unlike the RHO that observes it only for the forecasting interval.

In terms of the revenue from selling energy to the power grid R^{B2G}, case 3 sells 62.9 % more energy than case 2, whereas it's 0 in case 1 as discharging to the grid is excluded in this case. In general, it can be noticed that the income from selling energy to the grid is much lesser than that from the swapping service since the price of the swapping service is higher. Thus, it's very likely for the optimization solver to favor swapping over selling energy to the grid.

Case 3 resulted in a higher profit that is 18.7 % more than case 2 and the number of batteries swapped increased by 11.3% as well. It can be observed from Fig. 17 that the number of customers served in the RHO case is nearly the same as the unscheduled operation, however, RHO is economically better due to the benefits from discharging to the power grid. In conclusion, the comparison shows that the dynamic scheduling in case 3 outperforms cases 1 and 2.

B. Rolling Horizon Optimization Analysis

To highlight the characteristics of the RHO mechanism, the effect of different lengths of the prediction horizon has been considered. In Fig. 18, the output of different lengths of the rolling window is displayed to validate the robustness of this optimization technique with our proposed BSS framework. Furthermore, a perfect information solution of profit $2252 is

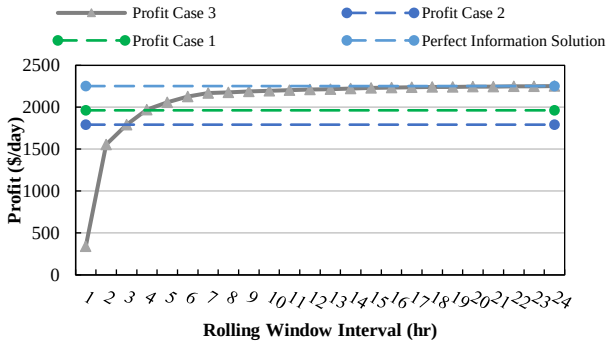

Fig. 18. The effect of the length of the rolling horizon on the BSS profit.

included at which the forecasting horizon is equal to the scheduling horizon. This solution is used as a reference as it indicates the highest profit that could be achieved using the RHO scheduling.

As shown in Fig. 18, the RHO scheduling (case 3) outperforms cases 1 and 2 when the forecasting horizon exceeds three hours. Furthermore, the sharp rise in the profit curve in the first few hours is due to the small prediction horizon. For instance, in a one-hour rolling window, all batteries tend to swap and discharge at the first iteration to maximize the profit. Hence, for the next iterations of the rolling window, one hour is not enough to replenish the energy of the batteries to generate profits within this window resulting in a small profit.

The longer the prediction horizon, the higher the daily profit obtained since more future information is available to solve the optimization problem. Finally, compared to the day-ahead scheduling the RHO scheduling results in an increased profit ranging between 10 % and 25.7 % depending on the length of the rolling horizon.

C. Policy Implications

For the BSS models to succeed, fast public and energy policies are required [36] – [37]. Therefore, we concluded our analysis with some policy implications that were proposed based on the obtained simulation results. Firstly, public policy action is required to encourage the development of the standards for the battery shape, mechanical insertion of batteries, and electrical connection. It's suggested that battery manufacturers unify a standard battery pack for each EV Company. Such that, for the same EV manufacturer, a small EV takes one pack, whereas, a large truck or a bus takes multiple packs.

Secondly, standards will be required for the swapping stations, for example, approved equipment will be crucial for consumer confidence since charged batteries must be sorted out as EV-ready (those that meet the applicable minimum standards), fit for reuse, or to be recycled. In this regard, the government should encourage stakeholders to work together. The charging equipment, on the other hand, must satisfy both the demand for electric vehicles and the grid limitations. In general, demonstration of the most appropriate of the various operating and regulatory models requires public policy.

In the end, the BSS technology leads to acceleration of transportation electrification allowing the mobility demand to become a flexible decarbonized power system with high power

and high storage capacity as well. This technology also increases energy efficiency since slower battery charging leads to lower energy losses and reduces battery degradation. This, together with the decarbonization of the power system makes the BSS a very attractive solution.

VII. Conclusion

Battery Swapping Stations (BSS) provide a fast alternative service compared to charging EVs at the charging stations. In this paper, a new model for the dynamic operation of the BSS is presented. The goal of the model is to provide optimal dynamic scheduling of the batteries at the BSS using an LSTM-based RHO mechanism. The batteries at the BSS are scheduled to operate in B2G, G2B, and B2B modes. Battery heterogeneity and the diversification of the EV types are adopted in this model. Hence, the battery management is unified which obviously achieved global gains. Furthermore, variable-rate chargers are used instead of traditional constant current chargers to fully utilize the grid services. Moreover, detailed modeling of the charging characteristics is considered. The optimization problem of the BSS is modeled as an MINLP then it's linearized into a MILP and solved using an exact optimization approach. The simulation results show that the proposed RHO dynamic scheduling offers economic benefits, ensures reliability, and is more robust to uncertainty. Compared with unscheduled and day-ahead operations, the dynamic RHO model of the BSS resulted in higher profits. Accordingly, the following conclusions are obtained:

- The operations scheduling of the BSS using the LSTM-based RHO mechanism increased the profit between 10% and 25.7% compared to the conventional scheduling methods
- The RHO mechanism can serve between 11% and 14% more customers than the conventional scheduling methods

As a result, the dynamic mechanism introduced in this paper outperforms the day-ahead scheduling approach and serves as future guidance for BSS operators. It's worth highlighting that, the work investigated in this research relies in its main operation on smart communication devices that communicate between the BSS control center, the swapping bays and the charging racks to achieve a fully automated swapping environment. In this regard, this system can be further enhanced by combining it with the connected vehicles technology in the intelligent transportation systems to collect real-time information on each EV, process it, and analyze it. Hence, providing more convenient services to BSSs and EV owners by efficiently relieving congestion on some routes and power plants. As a result, future research studies can focus on planning of several BSSs while considering the effect of traffic flow. Moreover, the allocation of the BSSs and their impact on the distribution networks can be investigated while considering uncertainties.

Appendix A
Li-ion Battery Degradation Model

The degradation in the battery SOC in our model is calculated as a function of the number of cycles [38]. The decrease in the SOC of a certain battery b when this battery encounters several charging cycles $\mathcal{C}_b$ is calculated as follows:

$$\Delta\text{soc}_b^{\text{deg}} = -8.954 \times 10^{-10} \times \mathcal{C}_b^3 + 7.883 \times 10^{-7} \times \mathcal{C}_b^2 - 2.814 \times 10^{-4} \times \mathcal{C}_b \qquad \forall b \in B, \tag{38}$$

Equation (39) approximates the number of charging cycles as the total number of swaps, such that a battery encounters a charging cycle before swapping with a DB. The summation of the binary variable $sw_{\tau,b,\beta}$ over all the swapping bays and the time T, results in the total number of swaps for battery b. Thus, we have

$$\mathcal{C}_b \cong \sum_{(\tau \in T)} \sum_{(\beta \in U)} sw_{\tau,b,\beta} \qquad \forall b \in B, \tag{39}$$

The degradation effect is added to the formulation by subtracting the degradation cost from the total revenue as shown in (1). The total daily degradation cost for all the batteries available at the BSS calculated in (40), as follows:

$$C^{DEG} = -\sum_{(b \in B)} 100\,\% \times \Delta\text{soc}_b^{deg} \times \mu_b^{deg} \tag{40}$$

where μ_b^{deg} is the degradation cost for each battery b.

Appendix B
Greedy Battery Swapping Algorithm

The greedy battery swapping algorithm is presented in Algorithm 2. This algorithm is described as a greedy algorithm as it's designed to swap batteries and charge the depleted ones as soon as possible. We implemented this algorithm in order to simulate the BSS unscheduled daily operation. The algorithm is mainly based on goal programming such that it solves the problem using two objective goals. The first goal is to maximize the revenue from swapping R^s while considering the actual EV arrivals at each time slot τ. Whereas, the second goal is to maximize the total charging power from all the batteries. The maximum number of batteries swapped $\mathcal{N}^{BAT-SW}$ is saved from

Algorithm. 2: greedy battery swapping algorithm

Input: Actual EV arrivals at each time slot τ
Output: Swapping and charging batteries as soon as possible

for τ = 1: 144 **do**
  goal 1:
    $OBJECTIVE \rightarrow \max_F(R^s)$
    subject to: Constraints (5) – (28)
    save the number of batteries swapped $\mathcal{N}^{BAT-SW}$
  terminate goal 1
  goal 2:
    fix $\mathcal{N}^{BAT-SW}$ in goal 2 with the value from goal 1
    $OBJECTIVE \rightarrow \max_F\left(\sum_{b \in B} p_{\tau,b}^{ch}\right)$,
    subject to: Constraints (5) – (28)
  terminate goal 2
  save F at time τ
end for

goal 1 to be fixed in goal 2, thus, ensuring maximum battery swapping at time τ. With this algorithm, we model the instantaneous actions taken by the BSS operator which are mainly maximizing the swapping revenue and charging all the possible DBs.

REFERENCES

[1] EEI celebrates 1 Million Electric Vehicles on U.S. Roads [online]. Available: https://www.eei.org/resourcesandmedia/newsroom, Accessed on: Jul. 19, 2021

[2] What are the challenges facing electric vehicle adoption [online]. Available:https://www.sgfleet.com/global/news/what-are-the-challenges-facing-electric-vehicle-adoption/, Accessed on: Jul. 19, 2021

[3] Osama M. Abdelwahab, Ahmed A. Shalaby, Mostafa F. Shaaban, "An optimal resource allocation for future parking lots with charger assignment considering uncertainties," in *Electric Power Systems Research*, vol. 200, 2021, 107455, ISSN 0378-7796.

[4] Tesla Models [online]. Available: https://www.tesla.com/model, Accessed on: Jul. 19, 2021

[5] X. Cheng *et al*., "Electrified Vehicles and the Smart Grid: The ITS Perspective," in *IEEE Transactions on Intelligent Transportation Systems*, vol. 15, no. 4, pp. 1388-1404, Aug. 2014.

[6] Y. Wang, W. Ding, L. Huang, Z. Wei, H. Liu and J. A. Stankovic, "Toward Urban Electric Taxi Systems in Smart Cities: The Battery Swapping Challenge," in *IEEE Transactions on Vehicular Technology*, vol. 67, no. 3, pp. 1946-1960, March 2018.

[7] Q. Dai, T. Cai, S. Duan and F. Zhao, "Stochastic Modeling and Forecasting of Load Demand for Electric Bus Battery-Swap Station," in *IEEE Transactions on Power Delivery*, vol. 29, no. 4, pp. 1909-1917, Aug. 2014.

[8] J. Lidicker, T. Lipman, and B.Williams, "Business model for subscription service for electric vehicles including battery swapping for SanFrancisco bay area, California," Transp. Res. Record: J. Transp. Res. Board, vol. 2252, pp. 83–90, 2011.

[9] H. Wu, G. K. H. Pang, K. L. Choy and H. Y. Lam, "An Optimization Model for Electric Vehicle Battery Charging at a Battery Swapping Station," in *IEEE Transactions on Vehicular Technology*, vol. 67, no. 2, pp. 881-895, Feb. 2018.

[10] A. A. Shalaby, M. F. Shaaban, M. Mokhtar, H. H. Zeineldin and E. F. El-Saadany, "Optimal Day-ahead Operation for a PV-based Battery Swapping Station for Electric Vehicles," *2021 6th International Symposium on Environment-Friendly Energies and Applications (EFEA)*, 2021, pp. 1-8.

[11] Y. Zheng, Z. Y. Dong, Y. Xu, K. Meng, J. H. Zhao and J. Qiu, "Electric Vehicle Battery Charging/Swap Stations in Distribution Systems: Comparison Study and Optimal Planning," in *IEEE Transactions on Power Systems*, vol. 29, no. 1, pp. 221-229, Jan. 2014.

[12] M. R. Sarker, H. Pandžić and M. A. Ortega-Vazquez, "Optimal Operation and Services Scheduling for an Electric Vehicle Battery Swapping Station," in *IEEE Transactions on Power Systems*, vol. 30, no. 2, pp. 901-910, March 2015.

[13] H. Liu, Y. Zhang, S. Ge, C. Gu and F. Li, "Day-Ahead Scheduling for an Electric Vehicle PV-Based Battery Swapping Station Considering the Dual Uncertainties," in *IEEE Access*, vol. 7, pp. 115625-115636, 2019.

[14] N. Liu, Q. Chen, X. Lu, J. Liu and J. Zhang, "A Charging Strategy for PV-Based Battery Switch Stations Considering Service Availability and Self-Consumption of PV Energy," in *IEEE Transactions on Industrial Electronics*, vol. 62, no. 8, pp. 4878-4889, Aug. 2015.

[15] S. Esmaeili, A. Anvari-Moghaddam and S. Jadid, "Optimal Operation Scheduling of a Microgrid Incorporating Battery Swapping Stations," in *IEEE Transactions on Power Systems*, vol. 34, no. 6, pp. 5063-5072, Nov. 2019.

[16] M. Ban, M. Shahidehpour, J. Yu and Z. Li, "A Cyber-Physical Energy Management System for Optimal Sizing and Operation of Networked Nanogrids With Battery Swapping Stations," in *IEEE Transactions on Sustainable Energy*, vol. 10, no. 1, pp. 491-502, Jan. 2019.

[17] X. Liu, T. Zhao, S. Yao, C. B. Soh and P. Wang, "Distributed Operation Management of Battery Swapping-Charging Systems," in *IEEE Trans. Smart Grid*, vol. 10, no. 5, pp. 5320-5333, Sept. 2019.

[18] X. Tan, G. Qu, B. Sun, N. Li and D. H. K. Tsang, "Optimal Scheduling of Battery Charging Station Serving Electric Vehicles Based on Battery Swapping," in *IEEE Transactions on Smart Grid*, vol. 10, no. 2, pp. 1372-1384, March 2019.

[19] S. Stüdli, W. Griggs, E. Crisostomi and R. Shorten, "On Optimality Criteria for Reverse Charging of Electric Vehicles," in *IEEE Transactions on Intelligent Transportation Systems*, vol. 15, no. 1, pp. 451-456, Feb. 2014.

[20] Q. Kang, J. Wang, M. Zhou and A. C. Ammari, "Centralized Charging Strategy and Scheduling Algorithm for Electric Vehicles Under a Battery Swapping Scenario," in *IEEE Transactions on Intelligent Transportation Systems*, vol. 17, no. 3, pp. 659-669, March 2016.

[21] R. Khodabakhsh and S. Sirouspour, "Optimal Control of Energy Storage in a Microgrid by Minimizing Conditional Value-at-Risk," in *IEEE Transactions on Sustainable Energy*, vol. 7, no. 3, pp. 1264-1273, July 2016.

[22] Peters, Diane L., Mechtenberg, Abigail R., Whitefoot, John, and Papalambros, Panos Y. "Model Predictive Control of a Microgrid With Plug-In Vehicles: Error Modeling and the Role of Prediction Horizon." *ASME 2011 Dynamic Systems and Control Conference and Bath/ASME Symposium on Fluid Power and Motion Control*, Volume 1. Arlington, Virginia, USA. October 31–November 2, 2011. pp. 787-794. ASME.

[23] A. O'Connell, A. Keane and D. Flynn, "Rolling multi-period optimization to control electric vehicle charging in distribution networks," *2014 IEEE PES General Meeting | Conference & Exposition*, 2014, pp. 1-1, doi: 10.1109/PESGM.2014.6938830.

[24] M. H. Amini, O. Karabasoglu, M. D. Ilić, K. G. Boroojeni and S. S. Iyengar, "ARIMA-based demand forecasting method considering probabilistic model of electric vehicles' parking lots," *2015 IEEE Power & Energy Society General Meeting, Denver*, CO, 2015, pp. 1-5.

[25] R. Khodabakhsh and S. Sirouspour, "Optimal Control of Energy Storage in a Microgrid by Minimizing Conditional Value-at-Risk," in *IEEE Transactions on Sustainable Energy*, vol. 7, no. 3, pp. 1264-1273, July 2016.

[26] J. Zhang, X. Mu, J. Fang and Y. Yang, "Time Series Imputation via Integration of Revealed Information Based on the Residual Shortcut Connection," in *IEEE Access*, vol. 7, pp. 102397-102405, 2019.

[27] L. Sehovac and K. Grolinger, "Deep Learning for Load Forecasting: Sequence to Sequence Recurrent Neural Networks With Attention," in *IEEE Access*, vol. 8, pp. 36411-36426, 2020.

[28] S. Siami-Namini, N. Tavakoli and A. Siami Namin, "A Comparison of ARIMA and LSTM in Forecasting Time Series," *2018 17th IEEE International Conference on Machine Learning and Applications (ICMLA)*, 2018, pp. 1394-1401, doi: 10.1109/ICMLA.2018.00227.

[29] X. Zhang, Y. Cao, L. Peng, N. Ahmad and L. Xu, "Towards Efficient Battery Swapping Service Operation Under Battery Heterogeneity," in *IEEE Transactions on Vehicular Technology*, vol. 69, no. 6, pp. 6107-6118, June 2020.

[30] A. A. Hussein, "Capacity fade estimation in electric vehicles Li-ion batteries using artificial neural networks," in 2013 *IEEE Energy Conversion Congress and Exposition*, 2013, pp. 677–681.

[31] M. A. Ortega-Vazquez, "Optimal scheduling of electric vehicle charging and vehicle-to-grid services at household level including battery degradation and price uncertainty," *IET Gener. Transm., Distrib.*, vol. 8, no. 6, pp. 1007–1016, Jun. 2014.

[32] Baek, S.; Lee, Y.H.; Park, S.H, "Centralized Ambulance Diversion Policy Using Rolling-Horizon Optimization Framework to Minimize Patient Tardiness," *Healthcare* 2020, *8*, 266.

[33] Hochreiter, S.; Schmidhuber, J. Long short-term memory. Neural Comput. 1997, 9, 1735–1780. [CrossRef].

[34] GAMS – A User's Guide [Online] Available: GAMS – A User's Guide [Online] Available: https://www.gams.com/latest/docs/gams.pdf, Accessed on: Jul. 19, 2021

[35] Time series forecasting using deep learning [online]. Available: https://www.mathworks.com/help/deeplearning/ug/time-series-forecasting-using-deep-learning.html, Accessed on: Jul. 19, 2021

[36] A.M. Vallera, P.M. Nunes, M.C. Brito, "Why we need battery swapping technology," *Energy Policy*, vol. 157, 2021, 112481.

[37] H. Wu, "A Survey of Battery Swapping Stations for Electric Vehicles: Operation Modes and Decision Scenarios," in IEEE Transactions on Intelligent Transportation Systems.

[38] G.K. Zaher, M.F. Shaaban, Mohamed Mokhtar, H.H. Zeineldin, "Optimal operation of battery exchange stations for electric vehicles," *Electric Power Systems Research*, vol. 192, 2021, 106935.

Ahmed A. Shalaby received the B.Sc. (Hons.) degree in electrical engineering from Ain Shams University, Cairo, Egypt, in 2018, and the M.Sc. degree in electrical engineering from the American University of Sharjah, Sharjah, United Arab Emirates, in 2021.
He is currently working toward the Ph.D. degree in the Department of Electrical and Computer Engineering, University of Alberta, Edmonton, AB, Canada. His current research interests include deep reinforcement learning applications to power systems, smart grid, renewable DG, distribution system planning, electric vehicles, and storage systems. He serves as a Reviewer for the IEEE TRANSACTIONS ON INTELLIGENT TRANSPORTATION SYSTEMS.

Mostafa F. Shaaban (SMIEEE) received the B.Sc. and M.Sc. degrees in electrical engineering from Ain Shams University, Cairo, Egypt, in 2004 and 2008, respectively, and the Ph.D. degree in electrical engineering from the University of Waterloo, Waterloo, ON, Canada, in 2014.
Currently, he is an associate professor in the Department of Electrical Engineering, American University in Sharjah, Sharjah, United Arab Emirates, and adjunct with University of Waterloo, Waterloo, ON, Canada. Dr. Shaaban has several publications in international journals and conferences and serves as an associate editor for IET smart grid and a reviewer for several refereed journals. His research interests include smart grid, renewable DG, distribution system planning, electric vehicles, storage systems, and bulk power system reliability.

Mohamed Mokhtar Received the B.Sc. (Hons.), M.Sc. and Ph.D degrees in electrical engineering from Ain Shams University, Cairo, Egypt, in 2010, 2014 and 2018, respectively. He is currently an assistant Professor with the Electrical Power and Machines Department, Faculty of Engineering, Ain Shams University. He has several publications in international journals and conferences and serves as a reviewer for several refereed journals. His research interests include the areas of modeling and control of power electronics converters, renewable generation, Electric Vehicles, Power System Reliability and dc microgrids.

Hatem Zeineldin (M'06–SM'13) received the B.Sc. and M.Sc. degrees in electrical engineering from Cairo University, Giza, Egypt, in 1999 and 2002, respectively, and the Ph.D. degree in electrical and computer engineering from the University of Waterloo, Waterloo, ON, Canada, in 2006. He was with Smith and Andersen Electrical Engineering, Inc., North York, ON, USA, where he was involved in projects involving distribution system designs, protection, and distributed generation. He was a Visiting Professor with the Massachusetts Institute of Technology, Cambridge, MA, USA. He is currently with Khalifa University, Abu Dhabi, UAE and on leave from the Faculty of Engineering, Cairo University, Egypt. His current research interests include distribution system protection, distributed generation, and micro grids. He is currently an Editor for the IEEE TRANSACTIONS ON ENERGY CONVERSION.

Ehab F. El-Saadany (F'18) IEEE Fellow for his contributions in distributed generation planning, operation and control. Professor in EECS Department at Khalifa University and Adjunct Professor at the ECE Department, University of Waterloo, Canada. Director of the Advanced Power and Energy Center (APEC). Received his BSc and MSc from Ain Shams University, Cairo, Egypt in 1986 and 1990, and his PhD from the University of Waterloo in 1998. Was with ECE at Waterloo between 2000 and 2019, where he was the Director of the Power MEng program between 2010 and 2015. An Internationally recognized expert in the area of sustainable energy integration and smart distribution systems. His research interests include smart grid operation and control, microgrids, self-healing, Cyber-Physical security of smart grids, protection, power quality, distributed generation and power electronics interfacing. He is an Editor of the IEEE TRANSACTIONS ON SMART GRID, the IEEE TRANSACTIONS ON POWER SYSTEMS, and IEEE Power Systems Letters. He is Registered Professional Engineer in the Province of Ontario.